Water Research 194 (2021) 116954

Contents lists available at ScienceDirect

Water Research

journal homepage: www.elsevier.com/locate/watres

Active DNRA and denitrification in oxic hypereutrophic waters

Elias Broman[a,b,*], Mindaugas Zilius[c], Aurelija Samuiloviene[c], Irma Vybernaite-Lubiene[c], Tobia Politi[c], Isabell Klawonn[d], Maren Voss[d], Francisco J.A. Nascimento[a,b], Stefano Bonaglia[a,c,e,f,*]

[a] Department of Ecology, Environment and Plant Sciences, Stockholm University, 106 91 Stockholm, Sweden
[b] Baltic Sea Centre, Stockholm University, 106 91 Stockholm, Sweden
[c] Marine Research Institute, Klaipeda University, 92294 Klaipeda, Lithuania
[d] Department of Biological Oceanography, Leibniz Institute for Baltic Sea Research Warnemünde, Seestr. 15, 18119 Rostock, Germany
[e] Department of Biology, University of Southern Denmark, 5230 Odense, Denmark
[f] Department of Marine Sciences, University of Gothenburg, Box 461, 405 30 Gothenburg, Sweden

ARTICLE INFO

Article history:
Received 20 December 2020
Revised 17 February 2021
Accepted 18 February 2021
Available online 21 February 2021

Keywords:
Cyanobacteria
Estuarine ecosystem
Eutrophication
Metagenome
Nitrogen cycling
Nutrients

ABSTRACT

Since the start of synthetic fertilizer production more than a hundred years ago, the coastal ocean has been exposed to increasing nutrient loading, which has led to eutrophication and extensive algal blooms. Such hypereutrophic waters might harbor anaerobic nitrogen (N) cycling processes due to low-oxygen microniches associated with abundant organic particles, but studies on nitrate reduction in coastal pelagic environments are scarce. Here, we report on ^{15}N isotope-labeling experiments, metagenome, and RT-qPCR data from a large hypereutrophic lagoon indicating that dissimilatory nitrate reduction to ammonium (DNRA) and denitrification were active processes, even though the bulk water was fully oxygenated (> 224 μM O_2). DNRA in the bottom water corresponded to 83% of whole-ecosystem DNRA (water + sediment), while denitrification was predominant in the sediment. Microbial taxa important for DNRA according to the metagenomic data were dominated by Bacteroidetes (genus *Parabacteroides*) and Proteobacteria (genus *Wolinella*), while denitrification was mainly associated with proteobacterial genera *Pseudomonas, Achromobacter*, and *Brucella*. The metagenomic and microscopy data suggest that these anaerobic processes were likely occurring in low-oxygen microniches related to extensive growth of filamentous cyanobacteria, including diazotrophic *Dolichospermum* and non-diazotrophic *Planktothrix*. By summing the total nitrate fluxes through DNRA and denitrification, it results that DNRA retains approximately one fifth (19%) of the fixed N that goes through the nitrate pool. This is noteworthy as DNRA represents thus a very important recycling mechanism for fixed N, which sustains algal proliferation and leads to further enhancement of eutrophication in these endangered ecosystems.

1. Introduction

Nitrogen (N) and phosphorus (P) are the main limiting nutrients for aquatic life (Canfield et al., 2010). With the start of synthetic fertilizer production more than a hundred years ago, coastal environments have received increasing inputs of dissolved N and P, which have led to cultural eutrophication and subsequent phytoplankton blooms (Howarth and Marino 2006). Mineralization of such planktonic material accelerates oxygen (O_2) consumption, which potentially leads to anoxia, especially in scarcely ventilated and stratified aquatic systems (Breitburg et al., 2018; Carpenter et al., 1998). Under these conditions P is quickly recycled through internal feedback, and diazotrophs such as bloom-forming cyanobacteria capable of N_2 fixation become the main source of biological N (Montoya et al., 2004). The arising conditions, in which the system presents nuisance algal blooms, low visibility (< 1.5 m) and extremely high (> 50 μg L^{-1}) chlorophyll *a* concentrations, are called hypereutrophic (Paerl et al., 2011).

Abbreviations: C_{org}, Organic carbon; DIN, Dissolved inorganic nitrogen; DIP, Dissolved inorganic phosphorus; DNRA, Dissimilatory nitrate reduction to ammonium; DON, Dissolved organic nitrogen; GeTMM, Gene length corrected trimmed mean of M-values; POC, Particulate organic carbon; PON, Particulate organic nitrogen; RT-qPCR, Quantitative reverse transcription PCR; TDN, Total dissolved nitrogen; TN, Total nitrogen.

* Corresponding author.
E-mail addresses: elias.broman@su.se (E. Broman), stefano.bonaglia@gu.se (S. Bonaglia).

https://doi.org/10.1016/j.watres.2021.116954

Under oxic conditions, nitrifying bacteria oxidize the fixed ammonium (NH_4^+) to nitrate (NO_3^-), which is further reduced to N_2 under anoxic conditions through denitrification and anaerobic ammonium oxidation (anammox) (Canfield et al., 2005). In addition to these two NO_3^--depending pathways, NO_3^- may be reduced by another metabolic process, the dissimilatory nitrate reduction to ammonium (DNRA), which recycles fixed N in the system. Laboratory reactor studies have demonstrated that this process is in competition for free NO_3^- with denitrification (van den Berg et al. 2015), and its activity may increase when organic carbon is in surplus over NO_3^- (i.e. a high C:NO_3^- ratio) (Kraft et al., 2014). Recent literature has also shown that this process is ubiquitous in multiple aquatic environments due to the presence of oxic-anoxic interfaces, where NO_3^- is supplied via the oxic interface, and together with the availability of electron donors (organic matter, sulfide, etc.) facilitate DNRA activity (e.g. Caffrey et al., 2019, Hellemann et al., 2020, Klawonn et al., 2015, Stief et al., 2018).

In eutrophic lakes and coastal waters, the strictly anaerobic NO_3^- reduction pathways are mostly constrained to the top mm sediment layers (Canfield et al., 2005). Because of the vast size of benthic ecosystems, the oxic-anoxic interface in sediments constitutes the largest N-loss environment on Earth (Seitzinger et al., 2006). Water column anoxia can also host intense anaerobic N-cycling processes when NO_3^- is available and NO_3^- reduction pathways move vertically from the sediment to the water column (e.g. Bonaglia et al., 2016). In addition to anoxic sediment and waters, DNRA and denitrification have also been described in a number of other anoxic microenvironments found on zooplankton carcasses (e.g. Stief et al., 2018) and phytoplankton aggregates (e.g. Klawonn et al., 2015). Bulk water incubation experiments aimed at quantifying rates of NO_3^- reduction have therefore generally focused on anoxic sulfidic waters (e.g. Brettar and Rheinheimer 1991), suboxic waters of oxygen minimum zones (e.g. Dalsgaard et al., 2003), and on Baltic Sea waters at the oxic-anoxic interface (Bonaglia et al., 2016). Except for a recent study reporting on coupled nitrification-denitrification associated with suspended sediment particles in riverine water (Xia et al., 2017), to our knowledge, studies quantifying NO_3^- reduction in oxic waters are still missing.

In order to bridge this gap, we carried out a combination of geochemical and molecular assessments of an array of aerobic and anaerobic N-cycling processes in a hypereutrophic model system, the Curonian Lagoon (Baltic Sea), which constitutes the largest lagoon in Europe. Due to external loading and internal nutrient cycling, this lagoon presents massive phytoplankton blooms throughout the summer and chlorophyll *a* concentrations well above 50 µg L^{-1} (Zilius et al., 2014). The water column might therefore contain anoxic microenvironments, making DNRA and denitrification possible even though the water column is oxygenated. We hypothesized that: (1) the lagoon oxic bottom waters have the potential for hosting active NO_3^- reduction processes; (2) in the highly organic and eutrophic waters, DNRA rates are higher than denitrification; and (3) sediment NO_3^- reduction is quantitatively higher than in the water column. We tested these hypotheses by applying a combination of ^{15}N incubation experiments, metagenomic analysis, and quantitative reverse transcription PCR (RT-qPCR) of both pelagic and benthic environments.

2. Material and methods

2.1. Field sampling

Water and sediment samples were collected on the 26th of August 2019 in the south–central half of the Curonian Lagoon (close to the resort town Nida, 55°17.2388′ N, 21°01.2898′ E; Fig. 1). This part of the lagoon has a 3.5 m water depth, a water renewal time of 190 days (annual mean), and the water is situated above fluffy, oxygen-depleted, and organic-rich sediment (Umgiesser et al., 2016; Zilius et al., 2014). During sampling, in situ temperature, oxygen and salinity profiles were measured in the water column using an YSI 460 multiprobe (Xylem; Fig. S1). In addition, vertical profiles of photosynthetically active radiation (PAR) were measured with a LI-192 underwater quantum sensor (LI-COR). Water samples were collected in triplicate, from the surface (~0.5 m depth) and bottom (~3 m depth) layers, using a 2 L Ruttner water sampler and transferred to: 1) sterilized 1 L amber borosilicate bottles for molecular and flow-cytometer analysis; 2) opaque 2 L HPDE bottles for chemical analyses of environmental variables; and 3) plastic 10 L tanks for measurements of nutrient transformation rates. Additional samples (40 mL) from both the surface and bottom layers were preserved in 50 mL centrifuge tubes with acetic Lugol's solution for microscopic phytoplankton counting. Finally, 200 L of bottom water was collected for preincubation and incubation procedures in the laboratory.

During sampling 16 large (i.d. 8 cm, 30 cm length) and 7 small (i.d. 4.6 cm, 25 cm length) intact sediment cores were collected using a hand-corer, within 50–150 m of the sampling station. The large cores were used for benthic net flux and NO_3^- reduction pro-

Fig. 1. Satellite image showing the Curonian Lagoon. The image was taken by the operational land imager (OLI) onboard Landsat-8 satellite on September 18, 2014. The samples were collected at a station (red circle) in the south-central part of the lagoon, just outside the resort town Nida. LT = Lithuania, RUS = Russia, with the black line denoting the border between the two countries. (For interpretation of the references to color in this figure legend, the reader is referred to the web version of this article.)

Table 1
Overview of the experimental activities carried out for quantifying different N-cycling pathways in the water column and sediment. Isotope additions denote target ^{15}N atom% ($^{15}N_2$) or concentrations ($^{15}NH_4^+$ and $^{15}NO_3^-$) in the incubation vessel. Substrate enrichments for the N_2 fixation experiments were estimated based on rationale provide in (Montoya et al., 1996).

Experiment	Sample type	Incubation conditions	Incubation vessel	Isotope addition	*n*
N_2 fixation	Surface Water	14 h light + 10 h dark	500 mL bottles	$^{15}N_2$ (5% ^{15}N atom)	3
N_2 fixation	Bottom Water	Dark	500 mL bottles	$^{15}N_2$ (5% ^{15}N atom)	3
NH_4^+ assimilation	Surface Water	Light	250 mL bottles	$^{15}NH_4^+$ (0.3 µM)	3
NH_4^+ assimilation	Surface Water	Dark	250 mL bottles	$^{15}NH_4^+$ (0.3 µM)	3
NH_4^+ assimilation	Bottom Water	Dark	250 mL bottles	$^{15}NH_4^+$ (0.3 µM)	3
Denitrification and DNRA	Bottom Water	Dark	1.3 L liners	$^{15}NO_3^-$ (15 µM)	4
O_2 respiration	Bottom Water	Dark	1.3 L liners	No addition	4
NH_4^+, NO_2^-, O_3^- production	Bottom Water	Dark	1.3 L liners	No addition	4
NH_4^+, NO_2^-, NO_3^- benthic flux	Sediment	Dark	Intact cores	No addition	16
Denitrification and DNRA	Sediment	Dark	Intact cores	$^{15}NO_3^-$ (30 µM)	8
Denitrification and DNRA	Sediment	Dark	Intact cores	$^{15}NO_3^-$ (15 µM)	8

cesses measurements, while the small cores were used for sediment characterization and nucleic acids extraction. All water and sediment samples were transported back to the laboratory within 1 hour on ice (except for the 10 and 25 L plastic tanks), and immediately analysed. Water and sediment cores collected in the field were used in various incubation experiments to quantify different N-cycling pathways (see Table 1 for an overview of these experiments).

2.2. Water column N_2 fixation experiment

Pelagic N_2 fixation was determined using the $^{15}N_2$ technique according to Montoya et al. (1996). The samples were filled without air bubbles into 500 mL transparent HDPE bottles, and through a gas-tight septum each sample received 0.5 mL $^{15}N_2$ (98% $^{15}N_2$, Sigma-Aldrich). As the isotopic equilibration takes up to several hours (Mohr et al., 2010) we incubated the samples for 24 h (Mulholland et al., 2012; Wannicke et al., 2018). Surface water samples ($n = 3$) were incubated in outdoor tanks at ambient irradiance (14 h light and 10 h dark), while bottom water samples ($n = 3$) were wrapped in aluminum foil as in situ irradiance was below 1% of surface PAR at these depths. Three controls (without $^{15}N_2$ tracer) each for the surface and bottom water were incubated in parallel. After incubation the suspended material was collected on pre-combusted (8 h at 450 °C) Advantec GF75 glass fiber filters (0.3 µm pore size) for particulate organic (PO)^{15}N analyses. N_2 fixation rates (µmol L^{-1} h^{-1}) were calculated following Montoya et al. (1996) as

$$N_2 \text{ fixation rate} = \frac{\text{at\% } ^{15}N \text{ PON} - \text{at\% } ^{15}N \text{ control}}{\text{at\% } ^{15}N\,N_2 - \text{at\% } ^{15}N \text{ control}} \times \frac{\text{PON}}{t} \quad (1)$$

where at% ^{15}N is the atom percentage of ^{15}N in the PON pool in ^{15}N-amended samples (*at% ^{15}N PON*) and in control samples (*at% ^{15}N control*), and in the dissolved N_2 pool (*at% ^{15}N N_2*), *PON* is the amount of particulate organic nitrogen and *t* is the incubation time. All samples were stored frozen until analysis. Volumetric rates of N_2 fixation were calculated by converting areal rates taking into account the depth of the water column and the thickness of each layer (Montoya et al., 1996).

2.3. Water column NH_4^+ assimilation experiment

Ammonium assimilation rates in the water column were conducted based on a method previously described by Bartl et al. (2018). Briefly, 27 × 250 mL polycarbonate bottles were filled with collected field water to the top, avoiding bubbles, sealed and assigned, in triplicates, to the following treatments: (a) 9 × bottom water in dark; (b) 9 × surface water in light; and (c) 9 × surface water in dark. A volume of 200 µL from a 312.5 µM $^{15}NH_4Cl$ stock solution (99% ^{15}N atom, Sigma-Aldrich) was injected to a final concentration of 0.3 µM $^{15}NH_4^+$ through the butyl septum. This was followed by short incubations with three time points T_0, T_1 (1.5 h), and T_2 (3 h). At each time point, bottles ($n = 3$) were sacrificed and 60–70 mL of water were filtered on a pre-combusted 25 mm Advantec GF75 glass fiber filters for PO^{15}N analyses. Filters were frozen at –20 °C until analysis. Additional aliquots of filtered water (15 mL) were frozen at –20 °C for nutrient analyses (see below).

Ammonium consumption rates were calculated following Glibert et al. (1982), Klawonn et al. (2019). During incubations, the $^{15}NH_4^+$ concentrations commonly decrease exponentially with time due to the concurrent assimilation of $^{15}NH_4^+$ and dilution through $^{14}NH_4^+$ regeneration. To account for this exponential decrease, we used a non-linear curve fitting

$$k = \frac{ln(C_t/C_0)}{t} \quad (2)$$

where C_t and C_0 are the $^{15}NH_4^+$ concentrations at time *t* and time zero, respectively. Note that we did not measure the $^{15}NH_4^+$ concentrations directly but calculated them as the difference between the initially added amount of $^{15}NH_4^+$ and the amount of ^{15}N in the PON at each time point. Since total NH_4^+ concentrations were not significantly different between time points (*t*-test, *p* range = 0.07–1.00), NH_4^+ consumption and remineralisation rates were similar, and calculated as $k \times \bar{C}$, with $\bar{C}$ as the mean NH_4^+ concentrations during incubations (Glibert et al., 1982). Since we used the amount of ^{15}N in the PON to calculate NH_4^+ consumption rates, those can be considered as NH_4^+ assimilation rates.

2.4. Water column nutrient transformation and NO_3^- reduction experiment

Eight large plexiglass cylinders (i.d. 8 cm, 30 cm length) filled with ~1.3 L of bottom water each were submerged into an incubation tank containing approximately 20 L of aerated collected field water and maintained at constant temperature (21.3 ± 0.2 °C). Two stirrer bars, driven by an external magnet at 40 rpm, were inserted in each cylinder approximately at 10 cm height distance to each other to avoid water stagnation during incubation.

A first incubation for oxygen consumption and nutrient transformation processes (NH_4^+, NO_3^-, NO_2^-) was conducted by sealing four of the cylinders with rubber stoppers, while avoiding bubbles. The incubation was conducted in the dark and lasted six hours, and before and at the end a 20 mL of aliquot was subsampled, filtered (GF-75 filters) and frozen at –20 °C for nutrient analysis. Dissolved O_2 was monitored with a pre-calibrated oxygen microsensor (OX-50 microsensor, Unisense A/S). A second incubation, using the other set of four cylinders, was performed to target NO_3^- reduction processes by means of the $^{15}NO_3^-$ tracer addition

technique. The water inside each cylinder was spiked with ^{15}N-NO_3^- from a stock solution (20 mM $Na^{15}NO_3$, 98% ^{15}N atom, Sigma Aldrich) to a final concentration of 15 µM ^{15}N. To calculate the exact isotopic enrichment, water samples for NO_3^- analysis were collected prior and after the isotope addition. At the start of the time-series incubation, the cylinders were sealed with gas-tight plastic lids, avoiding bubbles. At intervals of approximately 4 h, and over an incubation time of 8 h, the cores were sampled through the perforated lid using a glass syringe equipped with a Viton tubing. The water removed was replaced with new water from the tank and the dilution factor was considered in the calculations. From each core a 40 mL subsample was transferred to a 12 mL exetainer (Labco Ltd) containing 200 μL of 7 M $ZnCl_2$ for $^{15}NH_4^+$ and $^{15}N_2$ measurements, or filtered on a pre-combusted GF-75 filter that was frozen (–20 °C) for later $PO^{15}N$ analysis. Denitrification and DNRA rates were calculated according to Bonaglia et al. (2016):

$$Denitrification\ rate\ =\ {}^{30}N_{2r}\ /(F_{NO_3^-})^2 \quad (3)$$

$$DNRArate = {}^{15}NH_{4r}^+/\left(F_{NO_3^-}\right)^2 \quad (4)$$

where $^{30}N_{2r}$ is the production rate of labelled N_2; $^{15}NH_4{}^+{}_r$ is the production rate of labelled NH_4^+; and F_{NO3-} is the fraction of ^{15}N in the NO_3^- pool.

2.5. Benthic nutrient flux and NO_3^- reduction rate measurements

A total of 16 large sediment cores were submerged into an incubation tank containing 200 L of aerated collected field water kept at a constant temperature (21.3 ± 0.2 °C). Cores were left uncapped in the tank to allow for full water mixing between the water inside the cores and tank bottom water. A stirrer bar, driven by an external magnet at 40 rpm, was inserted to the water phase of each core approximately 15 cm above the sediment surface to avoid water stagnation during incubation. After preincubation overnight, a gas-tight lid was placed on each core and dark incubations started. Four cores were immediately uncapped and 40 mL water aliquots were collected from each, transferred into 12 mL Exetainers (Labco Ltd), and fixed with 200 µL of 7 M $ZnCl_2$ for further gas measurements. A second 40 mL water aliquot was filtered (GF-75 filters) into a plastic test tube and frozen immediately at –20 °C for dissolved N analyses (see 2.6 section for details). At 1 h time intervals, four cores were uncapped and subsampled for respective analysis. The cores were then returned back to tank for subsequent incubation.

The second incubation for NO_3^- reduction followed the rationale of the revised isotope pairing technique (r-IPT, Risgaard-Petersen et al., 2003). The overlying water inside each core was spiked with ^{15}N- NO_3^- from a stock solution (20 mM $Na^{15}NO_3$, 98% ^{15}N atom, Sigma Aldrich) to final concentrations of 15 µM ^{15}N (n = 8 cores) and 30 µM ^{15}N (n = 8 cores). To calculate the exact isotopic enrichment, water samples for NO_3^- analysis were collected prior and after the isotope addition. The two different $^{15}NO_3^-$ concentrations were used to validate the method assumptions and to test for anammox activity (Risgaard-Petersen et al., 2003). Since the resulting rates were not significantly different, assumptions were met, anammox activity disregarded and denitrification rates pooled. The cores were left uncapped for 45 min to allow enough time to establish a stable NO_3^- concentration in the surface layer of the sediment. At the start of the time-course incubation, all cores were capped with rubber stoppers and every 1.5 h, four cores (two per treatment) were sacrificed and sediments were gently mixed with the overlying water down to the depth of 5–10 cm. Thereafter, 20 mL aliquots of the slurry were transferred into 12 mL exetainers (Labco Ltd) and fixed with 200 μL of 7 M $ZnCl_2$ for $^{29}N_2$ and $^{30}N_2$ analysis. An additional 40 mL subsample was collected and treated with 1.3 M KCl, vigorously shaken for 30 min, centrifuged supernatant (3000 rpm for 10 min) was filtered, and frozen at –20 °C for analyses of the exchangeable NH_4^+ pool and the $^{15}NH_4^+$ fraction. All benthic rates were calculated following established protocols (Bonaglia et al., 2014).

2.6. Water analysis

Water samples were filtered (GF-75 filters) within 1.5 h of collection into 10 mL PE tubes for dissolved inorganic nutrient (NH_4^+, NO_2^-, NO_x^-, DIP) and 25 mL glass vials for organic nitrogen (DON) analysis, and frozen immediately (–20 °C). All dissolved inorganic nutrient concentrations from field sampling and experiments were determined with a continuous flow analyser (San^{++}, Skalar) using standard colorimetric methods (Grasshoff 1983). NO_3^- was calculated as the difference between NO_x^- and NO_2^-. Total dissolved nitrogen (TDN) was analysed by high temperature combustion at 680 °C, followed by the catalytic oxidation/NDIR method using a Shimadzu TOC 5000 analyser with a TN module. DON was calculated as the difference between TDN and DIN (NH_4^++NO_2^-+NO_3^-). 400 mL water samples for chlorophyll *a* were filtered through Whatman GF/F filters (pore size 0.7 µm) and extracted with 90% acetone (24 h at 4 °C) and measured by spectrophotometry (Jeffrey and Humphrey 1975; Parsons et al., 1984).

Dissolved O_2 was quantified from the O_2:Ar ratio measured by membrane inlet mass spectrometer (MIMS) at Ferrara University (Bay Instruments, Kana et al., 1994) and corrected for Ar concentration and solubility based on temperature and salinity (Colt 2012). The ^{15}N-atom% in the dissolved N_2 pool in samples from the N_2 fixation experiment was also estimated using MIMS. Isotopic samples for $^{29}N_2$ and $^{30}N_2$ production were analysed by gas chromatography-isotopic ratio mass spectrometry (GC-IRMS) at the University of Southern Denmark. $^{15}NH_4^+$ from the isotope pairing technique experiments were analysed by the same GC-IRMS after conversion of NH_4^+ to N_2 (De Brabandere et al. 2015) by the addition of alkaline hypobromite (Warembourg 1993). Filters for $PO^{15}N$ analyses were analysed with a continuous-flow isotope ratio mass spectrometer (IRMS; Delta S, Thermo-Finnigan) at the Leibniz Institute for Baltic Sea Research Warnemünde (IOW).

Phytoplankton samples for identification and biomass were analysed at magnifications of × 200 and × 400 using a LEICA DMI 3000 inverted microscope (Utermöhl 1958) according to HELCOM recommendations (HELCOM 1988). Phytoplankton biomass (mg L^{-1}) was calculated as described in Olenina et al. (2006). Samples for abundances of heterotrophic bacteria were prefiltered through a 50 µm size mesh and preserved in 0.25% glutaraldehyde (final concentration) and frozen at –80 °C until further analysis (Marie et al., 2005). Before analysis, samples were stained with SYBR Green I (Invitrogen) to a final concentration of 1:10,000 (Marie et al., 2005). The diluted samples were then analysed using a flow-cytometer (AccuriTM C6, DB Biosciences).

2.7. Sediment characteristics

One of the small sediment cores were used to measure sediment oxygen penetration depth, and three small cores were sliced (top 0–2 cm sediment layer) and used for bulk density (dry weight per unit volume), organic carbon (C_{org}), total N (TN), and its isotopic composition ($\delta^{13}C$, $\delta^{15}N$). Before slicing, three O_2 microprofiles with a 100 µm resolution were measured in one random selected core using a pre-calibrated Clark-type oxygen microelectrode (OX-50, Unisense A/S) mounted on a motorized micromanipulator (MM33, Unisense). Measurements were performed in the dark at in situ temperature (21 °C). An overlying water column of 2–3 cm was left in the sediment core and aerated by a flow of

atmospheric air to ensure sufficient water stirring during measurements. The oxygen penetration depth was defined as the depth at the bottom of the oxygen profile where [O_2] was < 0.3 μM, which is the detection limit of the microelectrode.

From each core the sliced sediment was homogenised (5 mL) and dried at 60 °C for 48 h. In a subsample of dry sediment (2.9–4.5 mg), C_{org} and TN content and their isotopic composition ($\delta^{13}C$, $\delta^{15}N$) were measured with a mass spectrometer (Delta V, Thermo Scientific) coupled to an element analyser (FlashEA 1112, Thermo Electron Corporation) at the Center for Physical Sciences and Technology, Vilnius, Lithuania. Before measurements the samples were acidified with 1 M HCl in order to remove carbonates.

2.8. Nucleic acids extraction, cDNA synthesis, and sequencing

Water samples collected from the surface (n = 3) and bottom water (n = 3) were filtered (200–300 mL) by gentle vacuum (0.3 bar) onto sequential 10 µm polycarbonate membrane (GE Healthcare) and 0.22 µm MCE membrane filters (Frisenette ApS). Filters were transferred into sterile 2 mL cryotubes, immediately frozen and stored at −80 °C until DNA and RNA extraction. The filters were combined for nucleic acid extraction to ensure the representation of the whole microbial community. Three small intact sediment cores were sliced (0–0.5 and 0.5–1.0 cm sediment surface layers, n = 3), homogenized, and subsampled with a sterile spatula in order to sample the sediment microbial community. Nucleic acids were then extracted from 0.65–0.85 g of sediment sample.

DNA was extracted and purified using the QIAamp Fast DNA Stool Mini Kit (QIAGEN) following the manufacturer's instructions. For the improvement of bacterial cell rupture, lysis temperature was increased to 90 °C and for increasing the final DNA concentration in the eluate, elution volume of 50 µL was used. Quantity and quality of the DNA was measured on a NanoDrop One spectrophotometer (ThermoFisher Scientific). Metagenome sequencing was prepared with the library kit SMARTer ThruPLEX (Takara Bio) and sequenced at SciLife laboratory in Stockholm, Sweden. All samples were sequenced together on one lane using the Illumina NovaSeq S-Prime platform with a 2 × 150 bp setup.

RNA extraction was conducted with an initial incubation using lysozyme (20 mg mL^{-1}) and mutanolysin (250 U mL^{-1}) for 90 min at 37 °C. After incubation, 1 mL of Trizol was added and the samples were subjected to four cycles of bead beating with glass beads (for 2 min) and resting on ice (for 3 min) followed by incubation at room temperature (for 5 min). Thereafter, samples were cleaned following the protocol by Samuiloviene et al. (2019). Additional, RNA cleaning was performed using the RNeasy Mini Kit (QIAGEN) according to protocol instructions. Any leftover DNA in the extracted RNA was removed using the TURBO DNase kit (Invitrogen) according to the manufacturer's instructions. Contamination with residual DNA was tested by PCR amplification of the V3 region of the 16S rRNA gene, using primer pair Probio_Uni (5'-CCTACGGGRSGCAGCAG-3') and Probio_Rev (5'-ATTACCGCGGCTGCT-3') by (Milani et al., 2013). cDNA was generated with random primers using a SuperScriptIII Reverse Transcriptase (Invitrogen) with 5 min at 25 °C, 50 min at 55 °C, and 15 min at 70 °C, and the quantity and quality were measured on a NanoDrop One spectrophotometer. The cDNA samples were kept at −20 °C until transcript quantification by RT-qPCR.

2.9. RT-qPCR

Four functional genes involved in N-cycling (*nirS, nrfA, amoA*, and *nifH*) were targeted for quantification of its transcript abundance using the synthesized cDNA from the extracted RNA. qPCR standards were prepared using DNA from reference bacterial strains and specific primers (Table S1). Each amplification for the qPCR standards was performed under the following conditions: 5 min initial denaturation at 94 °C; 35 cycles at, 94 °C for 30 s, specific annealing temperature of the primer set for 30 s (Table S1), 72 °C for 45 s, 72 °C for 10 min, using 11 μL of Platinum Green Hot Start 2X Master Mix (Invitrogen), 0.3 μM of each primer, 1.25 µg μL^{-1} of BSA and 2 µL of template in total volume of 22 μL. Amplification products were purified using PureLink PCR Purification Kit (Invitrogen), quantified using Qubit 3.0 (Invitrogen) and sequenced (BaseClear B.V) to confirm their identity. Ten-fold serial dilutions ranging from 10^3 to 10^7 of copy number of the standard were used in RT-qPCR reactions in triplicate to generate an external quantification standard.

RT-qPCR reactions were performed on the StepOnePlus Real Time PCR system (ABI 7900 HT Sequence Detection System, PE Biosystems) using optical grade 96-well plates. The reaction mixture (20 μL) contained 10 µL of SYBR Green master mix, 0.2 µM of respective forward and reverse primers (Table S1), 2 mM of $MgCl_2$, 1.25 µg μL^{-1} of BSA and 2 µL of diluted cDNA sample (diluted 1:100 to 0.1 ng μL^{-1} cDNA). The thermocycling conditions were as follows: 50 °C for 2 min; initial denaturation at 94 °C for 10 min; 40 cycles at 94 °C (30 s), primer annealing temperature (see Table S1 for each primer temperature; 1 min), 72 °C (2 min). Specificity for RT-qPCR reactions was tested with a melting curve analysis (60 °C–94 °C, with 0.3 °C ramp increment) in order to identify unspecific PCR products such as primer dimers or fragments with unexpected fragment lengths. Each sample was analysed in triplicate and the average Ct-value was used to calculate transcript copy numbers per sample (mL^{-1} for water or mg^{-1} for wet sediments). Triplicate no-template controls were included in each RT-qPCR assay.

2.10. Bioinformatic analysis

The metagenomic data was analysed according to Zilius et al., 2021 with the same software and options used (unless specified). Briefly, illumina adapters and Phi-X174 controls sequences were removed by using SeqPrep 1.2 (St John 2011) and by mapping reads against the PhiX genome using bowtie2 2.3.4.3 (Langmead and Salzberg 2012), respectively. The reads were quality trimmed using Trimmomatic 0.36 (Bolger et al., 2014) using command: "LEADING:20 TRAILING:20 MINLEN:100", which yielded final quality trimmed reads with an average length of 145 bp and 34.5 million reads (min: 25.4, max: 44.0).

The paired without unpaired (PwU) reads from trimmomatic were used with MEGAHIT 1.1.2 to construct a co-assembly (Li et al., 2016a) that consisted of 9,148,477 contigs with an average length of 705 bp (range 200–311,543 bp). This was followed by gene prediction and gene annotation using the PROKKA 1.12 software suit (Seemann 2014). PROKKA uses Prodigal 2.6.3 for gene prediction (Hyatt et al., 2010) and BLAST 2.6.0+ (Altschul et al., 1990) for annotation against the UniProtKB/Swiss-Prot database (database downloaded: 31 January 2019). The quality trimmed reads were mapped on the assembly using bowtie2 on default settings. htseq-count from the HTSeq python package 0.9.1 (Anders et al., 2015) were used to estimate mapped sequence counts, and data was normalized within and between samples as Gene length corrected Trimmed Mean of M-values (GeTMM) (Smid et al., 2018). The final metagenomic data consisted of 152,288 unique UniProtKB/Swiss-Prot identifiers and 43,533 unique genes. The UniProtKB identifiers were used on UniProt's website (function: Retrieve/ID mapping) to retrieve reference taxonomy, gene names, and protein names. The nitrogen metabolism pathway as shown on the KEGG website (2020–07–28) was used to determine prokaryotic genes involved in nitrogen cycling for further analysis.

The pipeline for taxonomic identification followed the Kraken2+Bracken2 protocol (with the same options) as described

in (Broman et al., 2020). In brief, all quality trimmed metagenome sequences were taxonomically classified using Kraken2 2.0.8 (Wood et al., 2019) against the NCBI RefSeq genome database (database downloaded: 1 January 2020), and relative abundances estimated on genus level using Bracken 2.5 (Lu et al., 2017). The final data were analysed in the software Explicet 2.10.5 (Robertson et al., 2013) and normalized as relative abundances (%). See Data S1 for a list of sample names, number of sequences yielded before and after quality trimming, read lengths, quality scores, and number of reads classified with Kraken2. The sequence data has been uploaded to the NCBI BioProject: PRJNA645809.

2.11. Statistics

Benthic fluxes/rates were calculated from the least square linear regression of the solute concentration against time. The slope of the linear regression multiplied by the incubation cylinder's water column height gave the net solute increase (positive flux) or decrease (negative flux) per time and area. Measured volumetric rates (μmol L^{-1} d^{-1}) from the water were converted to areal scales (mmol m^{-2} d^{-1}) taking into account the lagoon's water column depth and thickness of each layer: surface – 1 m and bottom – 2.5 m. Shannon's H alpha diversity was based on the RefSeq lowest classified taxonomic level (i.e. genera), and was analysed in Explicet by first sub-sampling counts to the lowest sample size (6,003,552 counts) followed by bootstrap × 100 (with the bootstrap mean being reported). One-Way ANOVA tests (Shapiro-Wilk and Levene's tests were used to confirm assumptions for ANOVA were met) were then used to test for differences in Shannon's H alpha diversity between water and sediment layers. Bray-Curtis beta diversity based on the RefSeq lowest classified taxonomic level (i.e. genera) was analysed in the software past 4.0 (Hammer et al., 2001) and statistically tested with PERMANOVA (9999 permutations) between water and sediment layers. Significance level was set at $P < 0.05$, and all data are shown as mean ± standard error.

3. Results

3.1. Characteristics of water column and sediment

During sampling, the surface and bottom water were oxygenated (181 and 81% saturation, respectively: Table 2 & Fig. S1). The water salinity was 0.3 and the pH ~9 (Fig. S1). The water temperature was ~25 °C in the surface and ~22 °C in the bottom. The depth of the euphotic zone (Z_{eu} = 1% of surface PAR) was 1.4 m (Fig. S1).

Based on data measured in the field, lagoon conditions were clearly hypereutrophic (Fig. 1) and the dissolved nutrient concentrations, phytoplankton biomass, and bacteria number were distributed evenly throughout the water column (Table 2). This was also indicated by chlorophyll *a* concentrations of 72 and 77 μg L^{-1} in the surface and bottom water, respectively. DIN concentrations (i.e. NH_4^+ and NO_x each < 1 μM) were low compared to DON (40–50 μM). N limitation was indicated by the very low calculated DIN:DIP ratio (< 6). The N_2-fixing cyanobacteria constituted 25% of the total phytoplankton biomass (both in surface and bottom water), with species belonging to the genus *Dolichospermum* spp. (formerly planktonic *Anabaena* (Li et al., 2016b)) having the highest abundance (Data S2). The most abundant non-diazotrophic cyanobacteria included species belonging to the genus *Planktothrix* (42% of total phytoplankton biomass; Data S2). The top 0–2 cm sediment layers were depleted in ^{13}C and enriched in ^{15}N ($\delta^{13}C$ = −31.2‰ and $\delta^{15}N$ = 5.8‰), and had a C_{org} content of ~13%. In the sediments surface oxygen penetrated 1.5 mm (Table 2).

Table 2
Measured in situ environmental variables in the surface (~0.5 m) and bottom water (~3 m), as well as the top 0–2 cm sediment surface. The values show the mean ± standard error based on three replicates (except biomass and POC (particulate organic carbon) – two samples).

	Layer	
Water column	Surface	Bottom
O_2 (μM) / (%)	473 / 181	224 / 81
NH_4^+ (μM)	0.78 ± 0.03	0.72 ± 0.03
NO_x^- (μM)	0.63 ± 0.01	0.66 ± 0.03
DON (μM)	46.95 ± 1.99	47.44 ± 1.73
DIP (μM)	0.25 ± 0.01	0.24 ± 0.01
DIN:DIP (molar)	5.6	5.8
C:N (molar)	7.22 ± 0.41	7.32 ± 0.39
POC (μM)	847–931	837–841
Chlorophyll *a* (μg L^{-1})	72.2 ± 1.7	77.6 ± 2.3
Biomass of N_2 fixing cyanobacteria (mg L^{-1})	4.1	3.9
Biomass of other phytoplankton (mg L^{-1})	12.5	11.8
Bacteria number (× 10^9 L^{-1})	3.0 ± 0.1	3.4 ± 0.1
Sediment	Top 0–2 cm	
O_2 penetration depth (mm)	1.5 ± 0.01	
C_{org} (%)	12.97 ± 0.30	
TN (%)	1.83 ± 0.09	
C:N (molar)	7.09 ± 0.19	
$\delta^{13}C$ (‰)	−31.20 ± 0.06	
$\delta^{15}N$ (‰)	5.83 ± 0.03	

Table 3
Measured nitrogen cycling processes from two set of incubations: 1) water column and 2) intact sediment cores with bottom water and sediment (i.e. sediment fluxes were measured). The water data has been upscaled from L^{-1} d^{-1} units to m^{-2} d^{-1} based on a 1 m surface water column and a 2.5 m deep bottom water column (see Table S2 for measured μmol L^{-1} d^{-1} values). The outline of the experiments that resulted in these rates, and number of replicates, are available in Table 1.

Measured process	Layer (mmol m^{-2} d^{-1})		
	Surface water	Bottom water	Sediment
N_2 fixation	2.44 ± 0.38	1.53 ± 0.20	
NH_4^+ assimilation	*17.04 ± 2.79	18.96 ± 1.67	
DNRA (NO_3^- to NH_4^+)		0.19 ± 0.02	0.04 ± 0.03
Denitrification (NO_3^- to N_2)		0.04 ± 0.00	0.95 ± 0.06
O_2 consumption		−210.39 ± 6.44	−49.27 ± 20.33
NH_4^+ flux		32.36 ± 7.96	2.78 ± 0.93
NO_2^- flux		0.19 ± 0.05	0.13 ± 0.03
NO_3^- flux		1.73 ± 0.55	0.52 ± 0.20

* NH_4^+ assimilation rates in the surface water are based on light and dark incubation values combined together based on a 14 h light and 10 h dark period. For more info see Table S2.

3.2. Nitrogen transformation rates

The incubation experiments showed that total lagoon O_2 consumption was ~4 times higher in the bottom water compared to the sediment surface (Table 3; for raw rates see Table S2). DIN was produced in both the bottom water and the sediment, with substantially higher rates in the bottom water. NH_4^+ production was 9.7-fold higher than NO_x^- in the bottom water (~34 compared to 3.5 mmol m^{-2} d^{-1}), while NH_4^+ assimilation rates were similar in the bottom and surface water (~18 mmol m^{-2} d^{-1}). Raw N2 fixation rate was four times higher in the surface water than in the bottom water (~2.4 compared to ~1.5 mmol m^{-2} d^{-1}; Table 3). Isotope labeling experiments with $^{15}NO_3^-$ indicated that both DNRA ($NO_3^- \rightarrow NH_4^+$) and denitrification ($NO_3^- \rightarrow N_2$) occurred in the oxygenated bottom water (255 μM O_2) and in the sediment surface (Table S2; Table 3; see Fig. S2 for oxygen concentrations measured during the incubations). DNRA rates were higher than denitrification rates in the bottom water (~0.19 compared to ~0.04 mmol m^{-2} d^{-1}; Table 3), while in the sediment

denitrification rates were higher than DNRA rates (~0.95 compared to 0.04 mmol m^{-2} d^{-1}; Table 3). The sum of the total NO_3^- reduction rates from DNRA and denitrification [(DNRA)/(DNRA + Denitrification) = (0.19 + 0.04)/((0.19 + 0.04) + (0.04 + 0.95)) = 18.9%] results in total DNRA accounting for approximately 19% of the fixed N undergoing NO_3^- reduction. From the DNRA and denitrification experiments our results also showed that the ^{15}N amount on filters (i.e., $PO^{15}N$) did not increase with time. Anammox activity was excluded since the ^{14}N-N_2 production in cores incubated at 15 µM $^{15}NO_3^-$ did not significantly differ from that in cores incubated at 30 µM $^{15}NO_3^-$ (Student's *t*-test, $t = -0.483$, $P = 0.640$).

3.3. Microbial community composition

The community composition, based on the Bray Curtis dissimilarity index, was not different between the surface ($n = 3$) and bottom water ($n = 3$) (PERMANOVA, df = 5, *pseudo-F* = 2.95, $P = 0.10$). Similarly, the alpha diversity was not significantly different between the surface and bottom water layer (6.3 ± 0.1 Shannon's H, $n = 3$ each layer, One-Way ANOVA, df = 5, $F = 2.48$, $P = 0.19$). Cyanobacteria had the highest relative abundance of all phyla in the water column (55.7 ± 0.0%, data for both surface and bottom water; Fig. 2), followed by Proteobacteria (23.1 ± 3.8%), and Actinobacteria (10.5 ± 0.0%). The top dominant genera in the water included *Planktothrix* (18.5 ± 1.4%), *Anabaena* (14.1 ± 0.7%), *Dolichospermum* (7.9 ± 0.5%), *Microcystis* (3.9 ± 0.5%), and *Pseudanabaena* (4.0 ± 0.3%) all belonging to Cyanobacteria (Fig. 3). Note that pelagic *Anabaena* species that has not been updated as *Dolichospermum* might be present in the NCBI RefSeq database. Most *Anabaena* detected in the water column are likely pelagic. Non-cyanobacterial genera with high relative abundances in the water included actinobacterial *Streptomyces* and *Planktophila*, gammaproteobacterial *Pseudomonas*, and betaproteobacterial *Burkholderia* (Fig. 3).

Based on the Bray Curtis dissimilarity index, the sediment had a different microbial community composition when compared to the water column (Bray Curtis, PERMANOVA, df = 11, *pseudo-F* = 319.1, $P = 0.0019$). Likewise, the sediment also had a higher alpha diversity (Shannon's H, 8.4 ± 0.01, data compared between all sediment ($n = 6$) and water samples ($n = 6$), One-Way ANOVA, df = 11, $F = 258.5$, $P < 0.001$). However, there was no difference in beta and alpha diversity between the two sliced sediment sections (0–0.5 cm and 0.5–1 cm). Phyla with the highest relative abundance in the sediment included Actinobacteria, Firmicutes, and Proteobacteria (classes Alpha, Beta, and Gamma; Fig. 2). Top dominant genera in the sediment included e.g. actinobacterial

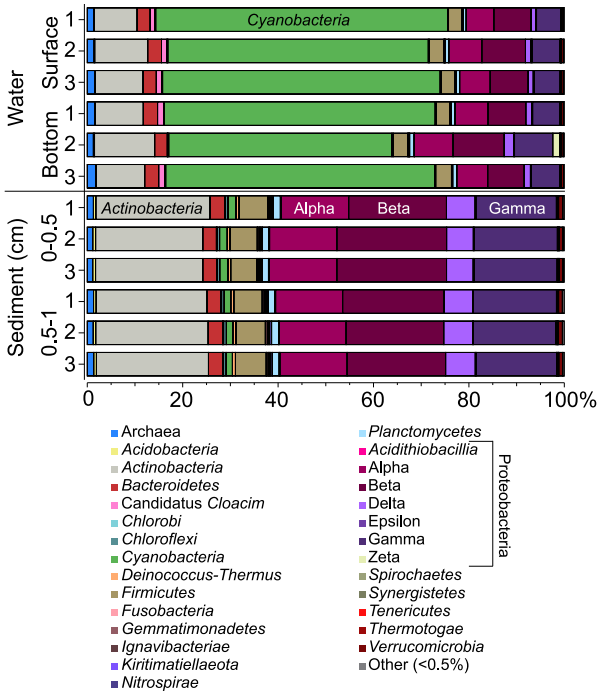

Fig. 2. Stacked bars showing Phyla with Proteobacteria divided into classes in the studied water and sediment layers (based on metagenomic data classified against the NCBI RefSeq database). Taxonomic groups less than 0.5% relative abundance (average of all samples) are grouped as "Other".

Streptomyces, gammaproteobacterial *Pseudomonas*, betaproteobacterial *Burkholderia* and *Cupriavidus*, and firmicutes *Thermobaculum* (Fig. S3). See Data S3 for a full list of classified taxa in the dataset.

3.4. N-cycling genes and transcripts

There were slightly more classified functional genes in the sediment (21,346 unique gene names including data from all samples) compared to the surface and bottom water samples (20,426 genes). See Data S4 for a full list of detected functional genes in the metagenomic dataset. The water column (surface and bottom, $n = 6$) contained more normalized counts for N-cycling genes compared to the sediment (238 GeTMM compared to 94 GeTMM in the sediment (both depth layers, $n = 6$) for the analysed genes; Fig. 4A). Considering the data was normalized for gene length and sequence depth (as GeTMM), this indicates that the func-

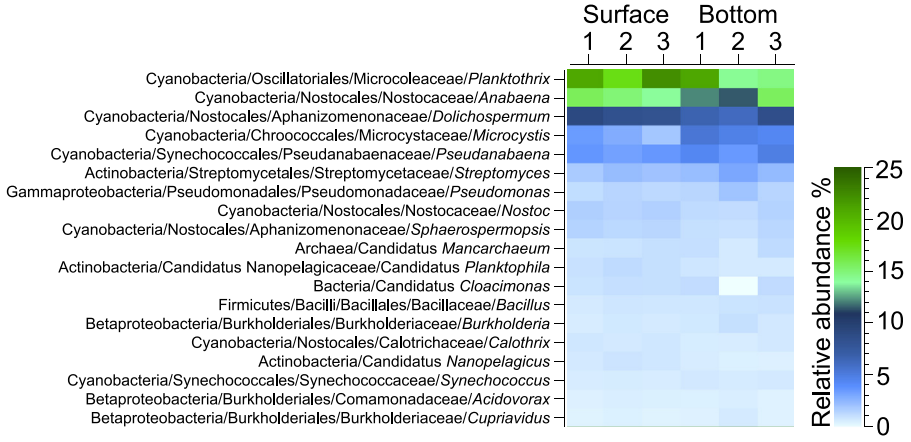

Fig. 3. The top dominant genera in the water column according to the metagenomic data (NCBI RefSeq database). The heatmap shows the lowest level of taxonomic classification (genera). The dataset was delimited to taxonomic groups > 0.5% relative abundance (average of all samples).

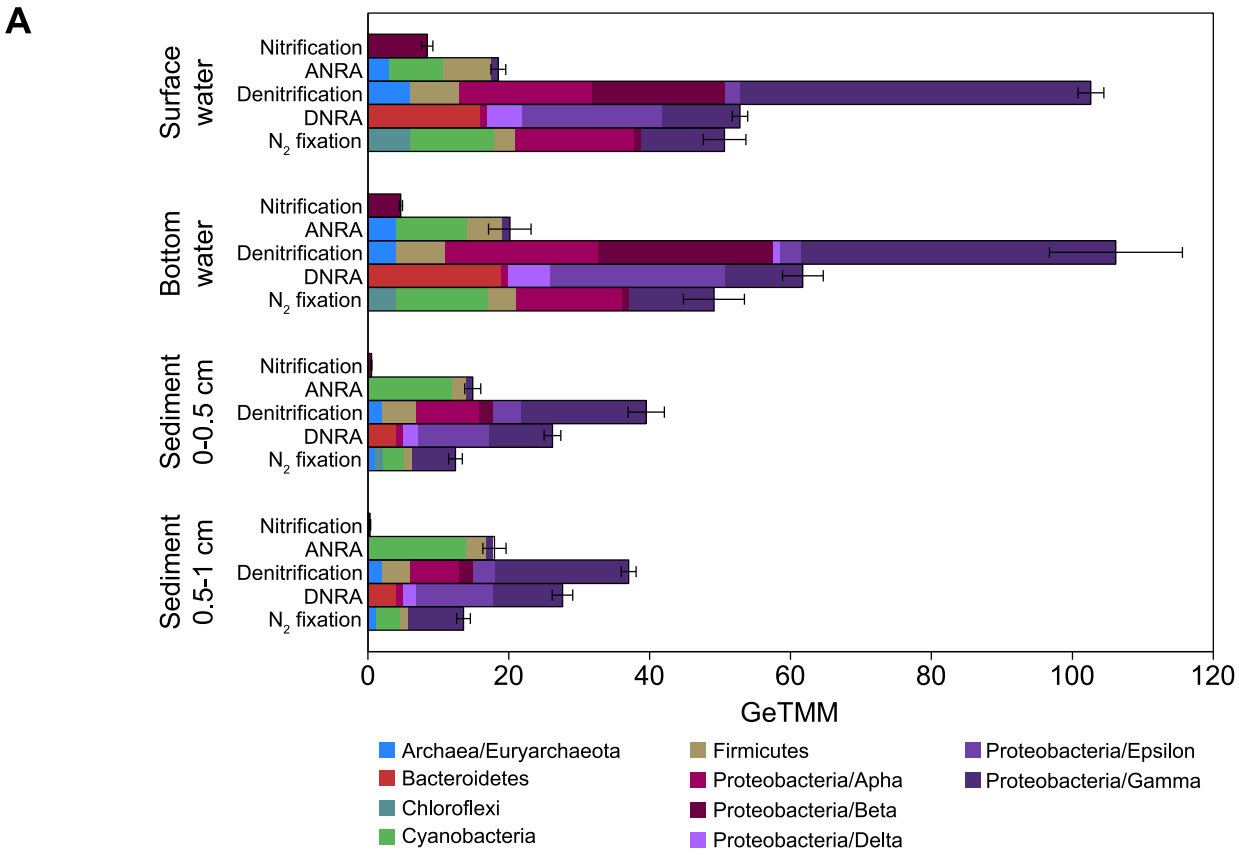

B

	Gene	Taxonomy (Phyla/Class/*Species*)	Surface Water 1	Surface Water 2	Surface Water 3	Bottom Water 1	Bottom Water 2	Bottom Water 3	Sediment 0-0.5 cm 1	Sediment 0-0.5 cm 2	Sediment 0-0.5 cm 3	Sediment 0.5-1 cm 1	Sediment 0.5-1 cm 2	Sediment 0.5-1 cm 3
DNRA	*nrfA*	Proteobacteria/Delta/*Desulfovibrio vulgaris*	5	5	4	5	6	5	2	2	2	2	2	2
	nrfA	Bacteroidetes/Bacteroidia/*Parabacteroides distasonis*	15	15	14	18	17	18	2	2	2	2	2	3
	nrfH	Proteobacteria/Epsilon/*Wolinella succinogenes*	21	21	19	25	25	24	9	10	10	9	10	11
	nirB	Proteobacteria/Gamma/*Pseudomonas stutzeri*	2	1	1	1	3	2	2	3	3	3	3	3
	nirB	Proteobacteria/Gamma/*Escherichia coli*	1	1	2	1	2	1	1	1	1	1	1	1
	nirD	Proteobacteria/Alpha/*Paracoccus denitrificans*	1	1	1	1	1	1	1	1	1	1	1	1
	nirD	Proteobacteria/Gamma/*Pseudomonas aeruginosa*	2	2	3	1	2	2	1	1	2	1	1	2
	nirD	Proteobacteria/Gamma/*Pseudomonas stutzeri*	5	5	4	3	5	5	3	3	3	3	3	3
Denitrification	*narG*	Firmicutes/Bacilli/*Bacillus subtilis*	3	5	3	4	6	4	1	1	2	1	1	2
	narG	Euryarchaeota/Halobacteria/*Haloferax mediterranei*	4	4	5	4	3	3	1	1	1	1	1	0
	narH	Proteobacteria/Gamma/*Shigella flexneri*	1	2	2	2	2	2	1	0	1	0	1	0
	narH	Proteobacteria/Gamma/*Escherichia coli*	4	3	3	4	5	2	2	2	2	3	2	2
	narI	Proteobacteria/Gamma/*Escherichia coli*	10	9	8	10	11	10	1	2	2	1	1	2
	napA	Firmicutes/Clostridia/*Symbiobacterium thermophilum*	3	2	2	2	2	2	1	2	2	1	1	1
	napA	Proteobacteria/Epsilon/*Nautilia profundicola*	1	2	1	2	3	1	2	1	2	2	2	2
	napB	Proteobacteria/Gamma/*Shigella flexneri*	3	3	3	3	4	2	2	1	2	1	2	2
	nirS	Proteobacteria/Gamma/*Pseudomonas aeruginosa*	12	9	10	12	12	8	4	3	4	4	4	5
	norB	Proteobacteria/Gamma/*Pseudomonas aeruginosa*	1	1	1	1	1	0	2	2	2	2	2	2
	norB	Proteobacteria/Gamma/*Pseudomonas stutzeri*	5	3	2	3	4	3	1	1	1	1	2	1
	norC	Proteobacteria/Gamma/*Pseudomonas stutzeri*	13	13	13	9	10	4	1	2	2	2	2	2
	nosZ	Proteobacteria/Alpha/*Bradyrhizobium diazoefficiens*	3	3	4	5	4	4	1	1	1	1	1	1
	nosZ	Proteobacteria/Alpha/*Brucella melitensis*	9	11	13	13	13	11	3	1	2	2	1	1
	nosZ	Proteobacteria/Alpha/*Rhizobium meliloti*	1	0	1	1	2	1	2	2	3	2	0	1
	nosZ	Proteobacteria/Beta/*Achromobacter cycloclastes*	10	11	9	18	13	12	1	0	0	1	0	1
	nosZ	Proteobacteria/Beta/*Cupriavidus necator*	5	6	4	6	4	5	1	0	1	0	1	0

GeTMM: 0 0 | 5 5 | ≥15 ≥15

Fig. 4. A) Distribution and taxonomy of selected N-cycling genes in the metagenomic data (based on UniProtKB/Swiss-Prot database). The y-axis shows different nitrogen metabolic processes in each sampled water or sediment layer, with: nitrification (genes *amoAB*); assimilatory nitrate reduction (ANRA, genes *narB, nosAB, nirA*); denitrification (genes *narGHI, napAB, nirKS, norBC, nosZ*); dissimilatory nitrate reduction (DNRA, genes *nirBD, nrfAH*); N_2 fixation (genes *nifDKH, vnfK*). The x-axis shows normalized sequence counts (GeTMM-values). The coloured stacked bars show the relative proportion (%) of the taxonomy, phyla, or proteobacteria classes attributed to the various metabolic processes. The error bars show the standard error ($n = 3$). B) DNRA and denitrification genes and their associated reference species in the UniProtKB database. The heatmap shows GeTMM-values (labels on dark cells have been coloured white). The dataset was delimited to database hits >1 GeTMM (average of all samples).

tional genes in the water column contained proportionally more N-cycling genes than the sediment. Denitrification genes (*narGHI, napAB, nirKS, norBC, nosZ*) were more prominent in the water column (surface + bottom, $n = 6$) when compared to the sediment (both sliced depths, $n = 6$) (104 ± 4 compared to 38 ± 1 GeTMM, df = 11, $F = 196.9$, $P < 0.01$; Fig. 4A). Similarly, DNRA genes (*nirBD* and *nrfAH*) also had more mapped reads in the water compared to the sediment (57 ± 2 compared 27 ± 1 GeTMM, df = 11, $F = 148.3$, $P < 0.01$; Fig. 4A). However, in contrast to denitrification that had no difference in GeTMM-values between the surface and bottom

Table 4
The table shows the RT-qPCR transcript copy numbers per 1 mL water or 1 mg sediment sample. The numbers in parenthesis behind the labels denote the biological replicate number (i.e. sediment core), and dashes in the table denote below detection limit. The studied genes code for denitrification (*nirS*), DNRA (*nrfA*), nitrification (*amoA*), and N_2 fixation (*nifH*).

Sample	Transcript copy numbers			
	nirS	*nrfA*	*amoA*	*nifH*
Surface water (1)	3916	3287	1006	831
Surface water (2)	1591	4265	1226	200
Surface water (3)	1252	2472	1072	–
Bottom water (1)	2716	32250	564	327
Bottom water (2)	–	–	–	54
Bottom water (3)	1369	62602	1098	91
Sediment 0–0.5 cm (1)	774	4806	380	14
Sediment 0–0.5 cm (2)	133	9058	468	18
Sediment 0–0.5 cm (3)	880	–	–	–
Sediment 0.5–1 cm (1)	1439	793	–	100
Sediment 0.5–1 cm (2)	9564	578	–	73
Sediment 0.5–1 cm (3)	–	–	–	65

water, DNRA had higher GeTMM-values in the bottom water (df = 5, $F = 7.7$, $P < 0.05$; Fig. 4A). Both of these processes were attributed to Proteobacteria classes Alpha, Beta, Delta, and Gamma. In addition, Firmicutes and the archaeal phyla Euryarchaeota were attributed to denitrification genes and Bacteroidetes to DNRA. Some examples of reference species in the UniProtKB database with the highest GeTMM-values attributed to DNRA genes included e.g. *Parabacteroides distasonis*, *Desulfovibrio vulgaris* and *Wolinella succinogenes* (Fig. 4B). Furthermore, the DNRA genes for these three species had higher GeTMM-values in surface and bottom water compared to the sediment (One-Way ANOVA with Tukey tests, df = 11, $F = 55–802$, $P < 0.05$). Species associated with denitrification genes included e.g. *Escherichia coli, Pseudomonas aeruginosa, Achromobacter cycloclastes*, and *Brucella melitensis* (Fig. 4B). These denitrification genes attributed to species also had higher GeTMM-values in the water when compared to the sediment (One-Way ANOVA with Tukey tests, df = 11, $F = 20–135$, $P < 0.05$). Assimilatory NO_3^- reduction genes (*narB, nosAB, nirA*) were attributed to Cyanobacteria, Firmicutes, and Euryarchaeota with no statistical difference between the water and sediment layers (18 ± 1 GeTMM for the whole dataset; Fig. 4A). N_2 fixation genes (*nifDKH* and *vnfK*) were more prominent in the water compared to the sediment (50 ± 2 compared to 13 ± 1 GeTMM, df = 11, $F = 238.8$, $P < 0.01$; Fig. 4A). However, there was no difference between the layers for N_2 fixation. In the water column, N_2 fixation genes were attributed to Chloroflexi, Cyanobacteria, Firmicutes, and Proteobacteria classes Alpha, Beta, and Gamma. This was different compared to the sediment, in which N_2 fixation genes were attributed to Euryarchaeota, Cyanobacteria, Firmicutes, and Gammaproteobacteria (Fig. 4A).

The RT-qPCR results showed that transcripts for *nirS, nrfA*, and *nifH* genes were present in all water and sediment layers, with the exception of the *amoA* transcript used in nitrification that was missing in the deeper anoxic 0.5–1 cm sediment layer (Table 4). Interestingly, the anaerobic process DNRA (gene *nrfA*, 3314 ± 518 transcripts per mL water) had significantly higher transcript numbers than nitrification (gene *amoA*, 1101 ± 65 transcripts; One-Way ANOVA, df = 5, $F = 18.4$, $P < 0.05$, $n = 3$) in the surface water. There was no significant difference between *nrfA* and *amoA* when compared to the denitrification gene *nirS* in the surface water. Finally, the bottom water was indicated to have the highest number of DNRA *nrfA* transcripts (32,250–62,602, $n = 2$) as well as *nirS* transcripts (1329–2716, $n = 2$; Table 4).

4. Discussion

4.1. Water column nitrate reduction processes

We found that the oxic bottom water of the hypereutrophic model system hosted NO_3^- reduction processes, with both active DNRA and denitrification. Similar findings have been reported from other pelagic coastal systems, but only after turning the water anoxic (Zeng et al., 2019). Consequently, apparent denitrification rates in the previous study (6–107 nmol L^{-1} h^{-1}) were 1–3 orders of magnitude higher than our measured rates (Table S2). To our knowledge, this is the first report of genuinely active water column NO_3^- reduction in shallow estuarine systems. By combining results from the isotope tracer experiments and flux measurements in the benthic and pelagic compartments, we were able to reconstruct the whole lagoon N-cycle (Fig. 5). Our data show that NO_3^- reduction in the water column was dominated by DNRA (83%), while in the sediment denitrification dominated (96%). Interestingly, whole-lagoon DNRA was estimated to retain 19% of the fixed N_2 that goes through the NO_3^- pool, intended as DNRA / (DNRA + denitrification). This highly organic and eutrophic estuarine system, with DNRA dominance over denitrification in the water column, differs from the deep anoxic basins of the open Baltic Sea, where denitrification is more prominent than DNRA (Bonaglia et al., 2016; Dalsgaard et al., 2013; Hietanen et al., 2012). The fact that water column DNRA was higher than denitrification might be explained by the very high C/NO_3^- ratio in the pelagic environment, which renders DNRA thermodynamically more favourable (Kraft et al., 2014; Tiedje et al., 1983).

All water column processes were measured at full O_2 saturation (255 μM O_2; Fig. S2). During stagnation events, when O_2 respiration exceeds its supply, bottom water can rapidly undergo hypoxia in the Curonian Lagoon (Fig. S4; Zilius et al. (2014)). Under hypoxia, the potential of the water column to significantly contribute to N-recycling and N-loss via DNRA and denitrification, respectively, will increase dramatically (Klawonn et al., 2015). Considering that the lagoon was N-limited and phytoplankton biomass was high, we cannot exclude that a portion of the added $^{15}NO_3^-$ was assimilated by the phytoplankton and re-mineralized to NH_4^+ (Klawonn et al., 2015). However, we have three lines of evidence against this possibility. First, we could not measure any $^{15}NO_3^-$ being incorporated into $PO^{15}N$. We acknowledge the fact that our $^{15}NO_3^-$ experiment was carried out in dark only, and thus we cannot exclude that minimal NO_3^- incorporation into $PO^{15}N$ might have happened in light conditions, but since the bottom waters of the lagoon are dark, we are confident that $^{15}NO_3^-$ was carried out dissimilatory. Second, we detected the highest amounts of *nrfA* RNA transcripts in the bottom water compared to surface water and sediment. These transcripts translate for a nitrite reductase enzyme used specifically in DNRA (Mohan et al., 2004). RNA transcripts have previously been observed for this gene in oxic waters in the hypereutrophic Lake Taihu, China (Krausfeldt et al., 2017). However, here we also conducted incubation experiments with $^{15}NO_3^-$ additions in both water and sediment to confirm that this was an active process. The NO_3^- reduction experiments indicated that DNRA activity was higher than denitrification in the bottom water, a pattern that was further confirmed by the higher number of *nrfA* transcripts compared to *nirS* ones. Third, the major players in these waters (*Planktothrix, Anabaena* and *Dolichospermum*) have never been shown, to our knowledge, to be able to carry out dark NO_3^- assimilation. Thus, interpreting our chemistry and molecular results together, we suggest that DNRA was an active process in the oxygenated lagoon waters. Our results thus imply that DNRA in the oxic waters can facilitate a complete NH_4^+ cycling: NH_4^+ uptake → mineralization/NH_4^+ release → nitrification to NO_3^- (not directly measured in our study but supported

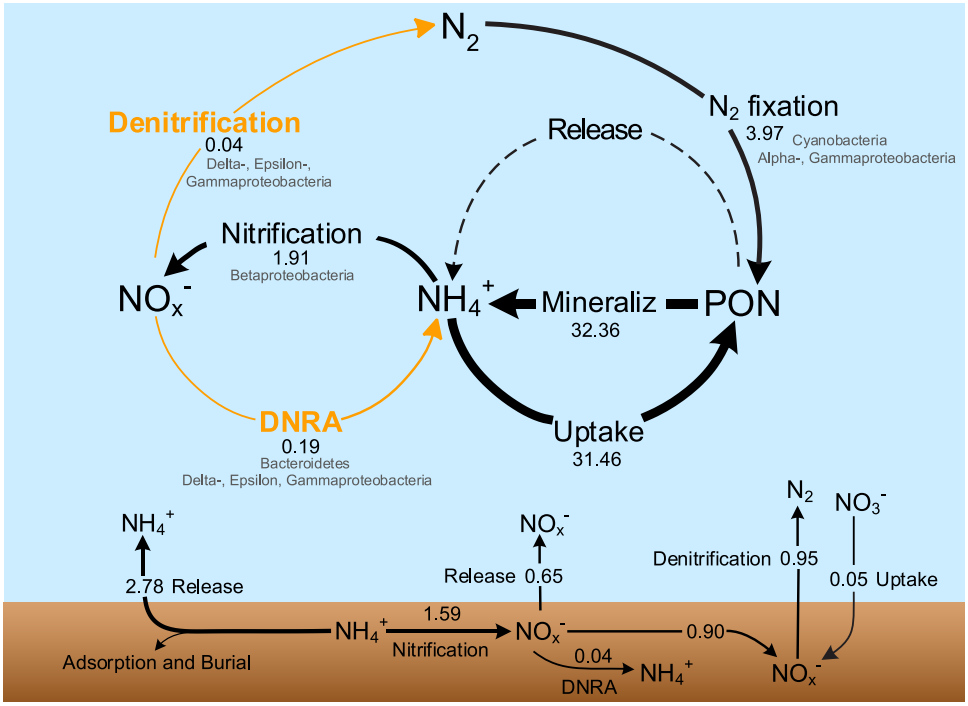

Fig. 5. The measured rates of N-cycling processes were used to calculate the whole water column and sediment fluxes. The bacterial phyla and proteobacteria classes associated with genes for specific processes were based on the most abundant groups in the metagenomic data. The values shown represent average rates in mmol m^{-2} d^{-1} and were calculated based on a 2.5 m aphotic bottom water column (except for N_2 fixation and NH_4^+ uptake that were measured both in surface and bottom water, and were therefore based on the whole 3.5 m water column). Pelagic nitrification rates were not directly measured in this study, and were estimated from production rates of NO_x^- from the flux experiments. Arrow thickness indicates the processes that had the highest measured rates, and the orange coloured arrows denote the novel water column nitrate reduction pathways, denitrification and DNRA. (For interpretation of the references to color in this figure legend, the reader is referred to the web version of this article.)

by the RT-qPCR *amoA* transcript data) → reduction to NH_4^+ via DNRA.

4.2. Pelagic niches for anaerobic process

The transcription of marker genes encoding for NO_3^- reduction and its derivatives typically occurs under low oxygen conditions (Härtig and Zumft 1999). In our study, this might have been associated with anoxic microniches on, e.g. zooplankton carcasses (Stief et al., 2018) and, most likely, on phytoplankton aggregates (Klawonn et al., 2015). Since the lagoon's water column was dominated by filamentous cyanobacteria, it is very likely that anoxic microniches were present inside cyanobacterial aggregates (Klawonn et al., 2015). We cannot exclude that denitrification and/or DNRA associated with suspended sediment particles (Xia et al., 2017) may have contributed to the measured rates. However, we consider the latter process negligible since the lagoon is an extremely low-energy ecosystem, which is characterized by stagnant conditions especially during summer months, with a water residence time of more than 4 months at the sampling site (Mėžinė et al., 2019).

Bacteria capable of DNRA are diverse and include, e.g. Bacteroidetes, Firmicutes and Proteobacteria (Mohan et al., 2004), which were also detected and attributed to DNRA in our metagenome data for both the water and sediment. Notably, Bacteroidetes were uniquely associated with DNRA genes compared to the other N-cycling pathways. Most of the DNRA genes were attributed to species *Parabacteroides distasonis* and *Wolinella succinogenes* in the UniProtKB database. *Parabacteroides distasonis* has been detected in e.g. the human gut (Ravcheev and Thiele 2014), and in an anaerobic industrial wastewater reactor amended with NO_3^- to promote DNRA and denitrification (Xie et al., 2015). *Wolinella succinogenes* is a known N-cycling bacterium capable of DNRA and reduction of N_2O to N_2 (Hollocher 1996; Luckmann et al., 2014). Moreover, members of Bacteroidetes are often found closely associated with filaments of cyanobacteria (Allgaier and Grossart 2006; Eigemann et al., 2019), likely benefiting from cyanobacterial exudates (Adam et al., 2016). Most of the denitrification genes were attributed to *Achromobacter cycloclastes* and *Pseudomonas aeruginosa*. Both *Pseudomonas aeruginosa* and *Achromobacter* sp. have been described capable of aerobic denitrification (Kathiravan and Krishnani 2014). In addition, the human pathogens *Brucella melitensis* and *E. coli* that have previously been detected in sediment and water (Zhou et al., 2019) were also found to be associated with the detected denitrification genes. Our results suggest that low oxygen or anoxic microniches associated with cyanobacteria and other algae might have been essential for DNRA and denitrification to function. Furthermore, our measured chlorophyll *a* values are in the same range as those reported for other hypereutrophic waters in, e.g. Asia (Paerl et al., 2011; Xing et al., 2005) and North America (Bigham et al., 2009; Norris and Laws 2017). Thus, our findings of active NO_3^- reduction in oxic waters are relevant for a large number of aquatic systems worldwide.

4.3. Recycling dominates over N_2 fixation

The *nifH* transcripts in our study indicated active diazotrophic communities in the water column and sediments. The highest N_2 fixation activity was measured in the surface water layer, where also the cyanobacterial biomass was higher, likely explained by enhanced growth due to photosynthesis (Castenholz 2015). Yet, we could detect relatively high N_2 fixation rates in the dark bottom water. More work is required to understand how long

these cyanobacteria can fix N_2 in dark conditions under high energetic cost. Due to gas vesicle and mixing events, heterocystous cyanobacteria can migrate upward to the surface layer (Walsby et al., 1995), where they can gain energy during photosynthesis.

Measured $\delta^{15}N$ (2.21‰) from living material and NH_4^+ uptake suggest that the pelagic communities of bacteria plus phytoplankton use a combined source of N for their growth, since the particulate organic nitrogen from N_2 alone would have a lower signal (ca. −2‰) (Voss et al., 1997). Our results show that N_2 fixation rates only partly (13%) meet nutritional needs for the microbial community (Fig. 5). However, up to 50% of this fixed N could be released as NH_4^+ (Adam et al., 2016). It seems likely that recycling of organic matter to NH_4^+ supplies the major amount of required N, which has previously been reported for other systems (see e.g. Présing et al., 2001), and recently also for the coastal Baltic Sea (Klawonn et al., 2019). Measured high NH_4^+ uptake rates and low standing concentration (< 1 µM) further indicate high turnover rates of NH_4^+ in the water column. We suggest that under N limitation, the lagoon efficiently fixes and recycles N via coupled N_2 fixation, organic matter oxidation, and assimilative processes. Thus, this recycling allows the conspicuous presence of non-fixing cyanobacteria (52% of total phytoplankton biomass) and other phytoplankton (23% biomass, based on microscopy counts; Data S2), which typically thrive in periods of higher inorganic N availability (Paerl and Otten 2013).

The study site is representative of 55% of the lagoon's surface water (Zilius et al., 2014), which allows for upscaling processes in a wider context including N inputs, removal, and recycling. The physical conditions are generally stable in the summer that lead to stratified waters, but strong wind events are observed in autumn and winter that cause resuspension (Mėžinė et al., 2019) making our extrapolation representative only for the summer period. In this area, pelagic N_2 fixation delivers 45% of the total N input (N_2 fixation, DIN release, and TN riverine input) during summer with intensive cyanobacterial blooms (July–September), assuming that the main tributary delivers 10,075 t of N (Zilius et al., 2018). Considering the denitrification rates, only 11% of N input (1133 t) is removed from the lagoon ecosystem. This is supported by a calculated low denitrification efficiency (22%) *sensu* Eyre and Ferguson (2009). Thus, the largest part of N is recycled in the system, including via DNRA in the water column.

5. Conclusions

We have shown that hypereutrophic oxygenated waters contain active DNRA and to a lesser extent denitrification, which were likely conducted in anoxic microniches related to the large growth of filamentous algae. Microbial genera associated with detected DNRA genes were predominated by *Parabacteroides* and *Wolinella*, while denitrification genes were associated with *Pseudomonas, Achromobacter,* and *Brucella*. With DNRA being active in the processing of nitrate reduction to the more bioavailable and less mobile ammonium, this process might sustain the growth of the pelagic community even further. Our data support the presence of a complete ammonium (re)cycling within the oxic waters of the lagoon, with clear implications for the enhancement of eutrophication. Since the conditions found in the studied lagoon (e.g. chlorophyll *a* concentrations) are similar to those found in other hypereutrophic systems (Bigham et al., 2009; Norris and Laws 2017; Paerl et al., 2011; Xing et al., 2005), we argue that our findings of active DNRA in oxic waters are relevant for a large number of aquatic systems worldwide. Enhanced water column DNRA might lower the capacity for these ecosystems to provide services such as water filtration, carbon sequestration, and fish supplies.

Contributions

MZ, SB designed the study; MZ, IVL, TP, SB sampled in the field; MZ, AS, IVL, TP, MV, SB conducted laboratory work; FN financed the sequencing and gave feedback on the manuscript; EB performed bioinformatics; EB, MZ, IK, SB analysed data; EB, MZ, IK, SB wrote the manuscript. All authors improved and approved the final manuscript.

Declaration of Competing Interest

The authors declare that they have no known competing financial interests or personal relationships that could have appeared to influence the work reported in this paper.

Acknowledgements

The authors acknowledge support from: "The role of atmospheric nitrogen fixation in the largest eutrophicated European lagoon (NitFix)" (Agreement No. P-MIP-17-126) grant under agreement with the Research Council of Lithuania (LMTLT); the Swedish Research Council Formas (Grant No. 2017-01513); the National Genomics Infrastructure in Stockholm funded by Science for Life Laboratory, the Knut and Alice Wallenberg Foundation and the Swedish Research Council; SNIC/Uppsala Multidisciplinary Center for Advanced Computational Science for assistance with massively parallel sequencing and access to the UPPMAX computational infrastructure. We thank Rūta Barisevičiūtė, Evelina Grinienė, Akvilė Kančauskaitė, Donata Overlingė, Iris Liskow for assistance in the laboratory, Diana Vaičiūtė for providing the remote sensing map, and Bo Thamdrup for making the GC-IRMS available at Nordcee. The manuscript was improved by addressing comments from two anonymous reviewers and the editor Mark van Loosdrecht.

Supplementary materials

Supplementary material associated with this article can be found, in the online version, at doi:10.1016/j.watres.2021.116954.

References

Adam, B., Klawonn, I., Svedén, J.B., Bergkvist, J., Nahar, N., Walve, J., Littmann, S., Whitehouse, M.J., Lavik, G., Kuypers, M.M., Ploug, H., 2016. N_2-fixation, ammonium release and N-transfer to the microbial and classical food web within a plankton community. ISME J. 10 (2), 450–459.

Allgaier, M., Grossart, H.-P., 2006. Seasonal dynamics and phylogenetic diversity of free-living and particle-associated bacterial communities in four lakes in northeastern Germany. Aquatic Microbial Ecology 45 (2), 115–128.

Altschul, S.F., Gish, W., Miller, W., Myers, E.W., Lipman, D.J., 1990. Basic local alignment search tool. J. Mol. Biol. 215 (3), 403–410.

Anders, S., Pyl, P.T., Huber, W., 2015. HTSeq–a Python framework to work with high-throughput sequencing data. Bioinformatics 31 (2), 166–169.

Bartl, I., Liskow, I., Schulz, K., Umlauf, L., Voss, M., 2018. River plume and bottom boundary layer–Hotspots for nitrification in a coastal bay? Estuar. Coast Shelf Sci. 208, 70–82.

Bigham, D.L., Hoyer, M.V., Canfield, D.E., 2009. Survey of toxic algal (microcystin) distribution in Florida lakes. Lake Reserv Manag. 25 (3), 264–275.

Bolger, A.M., Lohse, M., Usadel, B., 2014. Trimmomatic: a flexible trimmer for Illumina sequence data. Bioinformatics 30 (15), 2114–2120.

Bonaglia, S., Deutsch, B., Bartoli, M., Marchant, H.K., Brüchert, V., 2014. Seasonal oxygen, nitrogen and phosphorus benthic cycling along an impacted Baltic Sea estuary: regulation and spatial patterns. Biogeochemistry 119 (1), 139–160.

Bonaglia, S., Klawonn, I., De Brabandere, L., Deutsch, B., Thamdrup, B., Brüchert, V., 2016. Denitrification and DNRA at the Baltic Sea oxic–anoxic interface: substrate spectrum and kinetics. Limnol. Oceanogr. 61 (5), 1900–1915.

Breitburg, D., Levin, L.A., Oschlies, A., Grégoire, M., Chavez, F.P., Conley, D.J., Garçon, V., Gilbert, D., Gutiérrez, D., Isensee, K., Jacinto, G.S., Limburg, K.E., Montes, I., Naqvi, S.W.A., Pitcher, G.C., Rabalais, N.N., Roman, M.R., Rose, K.A., Seibel, B.A., Telszewski, M., Yasuhara, M., Zhang, J, 2018. Declining oxygen in the global ocean and coastal waters. Science 359 (6371), eaam7240.

Brettar, I., Rheinheimer, G., 1991. Denitrification in the Central Baltic: evidence for H_2S-oxidation as motor of denitrification at the oxic-anoxic interface. Mar. Ecol. Prog. Ser. 77 (2–3), 157–169.

Broman, E., Sun, X., Stranne, C., Salgado, M.G., Bonaglia, S., Geibel, M., Jakobsson, M., Norkko, A., Humborg, C., Nascimento, F.J.A, 2020. Low Abundance of Methanotrophs in Sediments of Shallow Boreal Coastal Zones With High Water Methane Concentrations. Front. Microbiol. 11 (1536).

Caffrey, J.M., Bonaglia, S., Conley, D.J., 2019. Short exposure to oxygen and sulfide alter nitrification, denitrification, and DNRA activity in seasonally hypoxic estuarine sediments. FEMS Microbiol. Lett. 366 (1).

Canfield, D.E., Glazer, A.N., Falkowski, P.G., 2010. The evolution and future of earth's nitrogen cycle. Science 330 (6001), 192–196.

Canfield, D.E., Kristensen, E. and Thamdrup, B. (2005) Aquatic Geomicrobiology. Canfield, D.E., Kristensen, E. and Thamdrup, B. (eds), Academic Press.

Carpenter, S.R., Caraco, N.F., Correll, D.L., Howarth, R.W., Sharpley, A.N., Smith, V.H., 1998. Nonpoint pollution of surface waters with phosphorus and nitrogen. Ecol. App. 8 (3), 559–568.

Castenholz, R.W., 2015. Bergey's Manual of Systematics of Archaea and Bacteria. John Wiley & Sons, Ltd.

Colt, J., 2012. Dissolved Gas Concentration in Water: Computation as Functions of Temperature. Salinity and Pressure, Elsevier.

Dalsgaard, T., Canfield, D.E., Petersen, J., Thamdrup, B., Acuna-Gonzalez, J., 2003. N_2 production by the anammox reaction in the anoxic water column of Golfo Dulce, Costa Rica. Nature 422 (6932), 606–608.

Dalsgaard, T., De Brabandere, L., Hall, P.O.J., 2013. Denitrification in the water column of the central Baltic Sea. Geochim. Cosmochim. Acta 106, 247–260.

De Brabandere, L., Bonaglia, S., Kononets, M., Viktorsson, L., Stigebrandt, A., Thamdrup, B., Hall, P.O.J., 2015. Oxygenation of an anoxic fjord basin strongly stimulates benthic denitrification and DNRA. Biogeochemistry 126 (1–2), 131–152.

Eigemann, F., Vogts, A., Voss, M., Zoccarato, L., Schulz-Vogt, H., 2019. Distinctive tasks of different cyanobacteria and associated bacteria in carbon as well as nitrogen fixation and cycling in a late stage Baltic Sea bloom. PLoS ONE 14 (12), e0223294.

Eyre, B.D., Ferguson, A.J.P, 2009. In: Nyborg, Denmark. Andersen, J.H., Conley, D.J. (Eds.), Eutrophication in Coastal Ecosystems: Towards better understanding and management strategies Selected Papers from the Second International Symposium on Research and Management of Eutrophication in Coastal Ecosystems, 20–23 June 2006. Springer, Netherlands, Dordrecht, pp. 137–146.

Glibert, P.M., Lipschultz, F., McCarthy, J.J., Altabet, M.A., 1982. Isotope dilution models of uptake and remineralization of ammonium by marine plankton. Limnology & Oceanography 27 (2), 639–650 (2).

Grasshoff, K. (1983) Methods of Seawater Analysis. Verlag Chemie, Weinheim, New York. Grasshoff, K., Kremling, K. and Ehrhardt, M. (eds).

Hammer, Ø., Harper, D.A.T., Ryan, P.D, 2001. PAST: paleontological statistics software package for education and data analysis. Palaeontol. Electron. 4 (1), 9.

HELCOM, 1988. Guidelines for the Baltic Monitoring Programme for the Third Stage, Part D. Biological Determinants. Baltic Marine Environment Protection Commission. Baltic Sea Envir. Proc 27.

Hellemann, D., Tallberg, P., Aalto, S., Bartoli, M., Hietanen, S., 2020. Seasonal cycle of benthic denitrification and DNRA in the aphotic coastal zone, northern Baltic Sea. Mar. Ecol. Prog. Ser. 637, 15–28.

Hietanen, S., Jäntti, H., Buizert, C., Jürgens, K., Labrenz, M., Voss, M., Kuparinen, J., 2012. Hypoxia and nitrogen processing in the Baltic Sea water column. Limnol. Oceanogr. 57 (1), 325–337.

Hollocher, T.C. (1996) Nitric Oxide. Lancaster, J. (ed), pp. 289–344, Academic Press, San Diego.

Howarth, R.W., Marino, R., 2006. Nitrogen as the limiting nutrient for eutrophication in coastal marine ecosystems: evolving views over three decades. Limnol. Oceanogr. 51 (1part2), 364–376.

Hyatt, D., Chen, G.L., Locascio, P.F., Land, M.L., Larimer, F.W., Hauser, L.J., 2010. Prodigal: prokaryotic gene recognition and translation initiation site identification. BMC Bioinformatics 11, 119.

Härtig, E., Zumft, W.G., 1999. Kinetics of nirS expression (cytochromecd 1 nitrite reductase) in Pseudomonas stutzeri during the transition from aerobic respiration to denitrification: evidence for a denitrification-specific nitrate-and nitrite-responsive regulatory system. J. Bacteriol. 181 (1), 161–166.

Jeffrey, S., Humphrey, G., 1975. New spectrophotometric equations for determining chlorophylls a, b, c1 and c2 in higher plants, algae and natural phytoplankton. Biochemie und physiologie der pflanzen 167 (2), 191–194.

Kana, T.M., Darkangelo, C., Hunt, M.D., Oldham, J.B., Bennett, G.E., Cornwell, J.C., 1994. Membrane inlet mass spectrometer for rapid high-precision determination of N2, O2, and Ar in environmental water samples. Anal. Chem. 66 (23), 4166–4170.

Kathiravan, V., Krishnani, K.K., 2014. *Pseudomonas aeruginosa* and *Achromobacter* sp.: nitrifying aerobic denitrifiers have a plasmid encoding for denitrifying functional genes. World J. Microbiol. Biotechnol. 30 (4), 1187–1198.

Klawonn, I., Bonaglia, S., Bruchert, V., Ploug, H., 2015. Aerobic and anaerobic nitrogen transformation processes in N_2-fixing cyanobacterial aggregates. ISME J. 9 (6), 1456–1466.

Klawonn, I., Bonaglia, S., Whitehouse, M.J., Littmann, S., Tienken, D., Kuypers, M.M.M., Brüchert, V., Ploug, H, 2019. Untangling hidden nutrient dynamics: rapid ammonium cycling and single-cell ammonium assimilation in marine plankton communities. ISME J. 13 (8), 1960–1974.

Kraft, B., Tegetmeyer, H.E., Sharma, R., Klotz, M.G., Ferdelman, T.G., Hettich, R.L., Geelhoed, J.S., Strous, M., 2014. The environmental controls that govern the end product of bacterial nitrate respiration. Science 345 (6197), 676–679.

Krausfeldt, L.E., Tang, X., van de Kamp, J., Gao, G., Bodrossy, L., Boyer, G.L., Wilhelm, S.W., 2017. Spatial and temporal variability in the nitrogen cyclers of hypereutrophic Lake Taihu. FEMS Microbiol. Ecol. 93 (4).

Langmead, B., Salzberg, S.L., 2012. Fast gapped-read alignment with Bowtie 2. Nat. Methods 9, 357.

Li, D., Luo, R., Liu, C.M., Leung, C.M., Ting, H.F., Sadakane, K., Yamashita, H., Lam, T.W., 2016a. MEGAHIT v1.0: a fast and scalable metagenome assembler driven by advanced methodologies and community practices. Methods 102, 3–11.

Li, X., Dreher, T.W., Li, R., 2016b. An overview of diversity, occurrence, genetics and toxin production of bloom-forming *Dolichospermum* (*Anabaena*) species. Harmful Algae 54, 54–68.

Lu, J., Breitwieser, F.P., Thielen, P., Salzberg, S.L., 2017. Bracken: estimating species abundance in metagenomics data. Peer J. Comput. Sci. 3, e104.

Luckmann, M., Mania, D., Kern, M., Bakken, L.R., Frostegård, Å., Simon, J., 2014. Production and consumption of nitrous oxide in nitrate-ammonifying Wolinella succinogenes cells. Microbiology 160 (8), 1749–1759.

Marie, D., Simon, N., Vaulot, D, 2005. Phytoplankton cell counting by flow cytometry. Algal Culturing Techniques 1, 253–267.

Mėžinė, J., Ferrarin, C., Vaičiūtė, D., Idzelytė, R., Zemlys, P., Umgiesser, G., 2019. Sediment transport mechanisms in a lagoon with high river discharge and sediment loading. Water (Basel) 11 (10), 1970.

Milani, C., Hevia, A., Foroni, E., Duranti, S., Turroni, F., Lugli, G.A., Sanchez, B., Martín, R., Gueimonde, M., van Sinderen, D., Margolles, A., Ventura, M., 2013. Assessing the Fecal Microbiota: an Optimized Ion Torrent 16S rRNA Gene-Based Analysis Protocol. PLoS ONE 8 (7), e68739.

Mohan, S.B., Schmid, M., Jetten, M., Cole, J., 2004. Detection and widespread distribution of the nrfA gene encoding nitrite reduction to ammonia, a short circuit in the biological nitrogen cycle that competes with denitrification. FEMS Microbiol. Ecol. 49 (3), 433–443.

Mohr, W., Grosskopf, T., Wallace, D.W., LaRoche, J., 2010. Methodological underestimation of oceanic nitrogen fixation rates. PLoS ONE 5 (9).

Montoya, J.P., Holl, C.M., Zehr, J.P., Hansen, A., Villareal, T.A., Capone, D.G., 2004. High rates of N 2 fixation by unicellular diazotrophs in the oligotrophic Pacific Ocean. Nature 430 (7003), 1027–1031.

Montoya, J.P., Voss, M., Kahler, P., Capone, D.G., 1996. A Simple, High-Precision, High-Sensitivity Tracer Assay for N (inf2) Fixation. Appl. Environ. Microbiol. 62 (3), 986–993.

Mulholland, M., Bernhardt, P., Blanco-Garcia, J., Mannino, A., Hyde, K., Mondragon, E., Turk, K., Moisander, P., Zehr, J., 2012. Rates of dinitrogen fixation and the abundance of diazotrophs in North American coastal waters between Cape Hatteras and Georges Bank. Limnol. Oceanogr. 57 (4), 1067–1083.

Norris, B., Laws, E.A., 2017. Nutrients and phytoplankton in a shallow, hypereutrophic urban lake: prospects for restoration. Water (Basel) 9 (6), 431.

Olenina, I., Hajdu, S., Edler, L., Andersson, A., Wasmund, N., Busch, S., Göbe, J., Gromisz, S., Huseby, S., Huttunen, M., Jaanus, A., Kokkonen, P., Ledaine, I., Niemkiewicz, E., 2006. Biovolumes and size-classes of phytoplankton in the Baltic Sea. HELCOM Balt.Sea Environ. Proc. No (106).

Paerl, H.W., Otten, T.G., 2013. Harmful cyanobacterial blooms: causes, consequences, and controls. Microb. Ecol. 65 (4), 995–1010.

Paerl, H.W., Xu, H., McCarthy, M.J., Zhu, G., Qin, B., Li, Y., Gardner, W.S., 2011. Controlling harmful cyanobacterial blooms in a hyper-eutrophic lake (Lake Taihu, China): the need for a dual nutrient (N & P) management strategy. Water Res. 45 (5), 1973–1983.

Parsons, T., Maita, Y., Lalli, C.M., 1984. A Manual of Chemical and Biological Methods For Seawater Analysis. A Manual of Chemical and Biological Methods For Seawater Analysis. Pergamon Press.

Présing, M., Herodek, S., Preston, T., Vörös, L., 2001. Nitrogen uptake and the importance of internal nitrogen loading in Lake Balaton. Freshw. Biol. 46 (1), 125–139.

Ravcheev, D.A., Thiele, I., 2014. Systematic genomic analysis reveals the complementary aerobic and anaerobic respiration capacities of the human gut microbiota. Front. Microbiol. 5, 674 -674.

Risgaard-Petersen, N., Nielsen, L.P., Rysgaard, S., Dalsgaard, T., Meyer, R.L., 2003. Application of the isotope pairing technique in sediments where anammox and denitrification coexist. Limnol. Oceanography 1 (1), 63–73.

Robertson, C.E., Harris, J.K., Wagner, B.D., Granger, D., Browne, K., Tatem, B., Feazel, L.M., Park, K., Pace, N.R., Frank, D.N., 2013. Explicet: graphical user interface software for metadata-driven management, analysis and visualization of microbiome data. Bioinformatics 29 (23), 3100–3101.

Samuiloviene, A., Bartoli, M., Bonaglia, S., Cardini, U., Vybernaite-Lubiene, I., Marzocchi, U., Petkuviene, J., Politi, T., Zaiko, A., Zilius, M., 2019. The effect of chironomid larvae on nitrogen cycling and microbial communities in soft sediments. Water 11 (9), 1931.

Seemann, T., 2014. Prokka: rapid prokaryotic genome annotation. Bioinformatics 30 (14), 2068–2069.

Seitzinger, S., Harrison, J.A., Bohlke, J.K., Bouwman, A.F., Lowrance, R., Peterson, B., Tobias, C., Van Drecht, G., 2006. Denitrification across landscapes and waterscapes: a synthesis. Ecol. App. 16 (6), 2064–2090.

Smid, M., Coebergh van den Braak, R.R.J., van de Werken, H.J.G., van Riet, J., van Galen, A., de Weerd, V., van der Vlugt-Daane, M., Bril, S.I., Lalmahomed, Z.S., Kloosterman, W.P., Wilting, S.M., Foekens, J.A., IJzermans, J.N.M., Coene, P.P.L.O., Dekker, J.W.T., Zimmerman, D.D.E., Tetteroo, G.W.M., Vles, W.J., Vrijland, W.W., Torenbeek, R., Kliffen, M., Carel Meijer, J.H., vd Wurff, A.A., Martens, J.W.M., Sieuwerts, A.M. and Bioinformatics, o.b.o.t.M.s.g.J.B. (2018) Gene length corrected trimmed mean of M-values (GeTMM) processing of RNA-seq data performs similarly in intersample analyses while improving intrasample comparisons. 19(1), 236.

St John, J. (2011) SeqPrep. https://github.com/jstjohn/SeqPrep.

Stief, P., Lundgaard, A.S.B., Treusch, A.H., Thamdrup, B., Grossart, H.-P., Glud, R.N, 2018. Freshwater copepod carcasses as pelagic microsites of dissimilatory nitrate reduction to ammonium. FEMS Microbiol. Ecol. 94 (10), fiy144.
Tiedje, J.M., Sexstone, A.J., Myrold, D.D., Robinson, J.A., 1983. Denitrification: ecological niches, competition and survival. Antonie Van Leeuwenhoek 48 (6), 569–583.
Umgiesser, G., Zemlys, P., Erturk, A., Razinkova-Baziukas, A., Mežine, J., Ferrarin, C., 2016. Seasonal renewal time variability in the Curonian Lagoon caused by atmospheric and hydrographical forcing. Ocean Sci. 12, 391–402.
Utermöhl, H., 1958. Zur vervollkommnung der quantitativen phytoplankton-methodik: mit 1 Tabelle und 15 abbildungen im Text und auf 1 Tafel. Internationale Vereinigung für theoretische und angewandte Limnologie: Mitteilungen 9 (1), 1–38.
Walsby, A.E., Hayes, P.K., Boje, R., 1995. The gas vesicles, buoyancy and vertical distribution of cyanobacteria in the Baltic Sea. Eur. J. Phycol. 30 (2), 87–94.
van den Berg, E.M., van Dongen, U., Abbas, B., van Loosdrecht, M.C.M., 2015. Enrichment of DNRA bacteria in a continuous culture. ISME J. 9 (10), 2153–2161.
Wannicke, N., Benavides, M., Dalsgaard, T., Dippner, J.W., Montoya, J.P., Voss, M., 2018. New perspectives on nitrogen fixation measurements using $^{15}N_2$ gas. Front. Mar. Sci. 5, 120.
Warembourg, F.R. (1993) Nitrogen Isotope Techniques. Knowles, R. and Blackburn, T.H. (eds), pp. 127–156, Academic Press San Diego,, USA.
Wood, D.E., Lu, J., Langmead, B., 2019. Improved metagenomic analysis with Kraken 2. Genome Biol. 20 (1), 257.
Voss, M., Nausch, G., Montoya, J., P., 1997. Nitrogen stable isotope dynamics in the central Baltic Sea: influence of deep-water renewal on the N-cycle changes. Mar. Ecol. Prog. Ser. 158, 11–21.
Xia, X., Jia, Z., Liu, T., Zhang, S., Zhang, L., 2017. Coupled Nitrification-Denitrification Caused by Suspended Sediment (SPS) in Rivers: importance of SPS Size and Composition. Environ. Sci. Technol. 51 (1), 212–221.
Xie, L., Ji, C., Wang, R., Zhou, Q., 2015. Nitrate reduction pathway in an anaerobic acidification reactor and its effect on acid fermentation. J. Biosci. Bioeng. 119 (1), 95–100.
Xing, Y., Xie, P., Yang, H., Ni, L., Wang, Y., Rong, K., 2005. Methane and carbon dioxide fluxes from a shallow hypereutrophic subtropical Lake in China. Atmos. Environ. 39 (30), 5532–5540.
Zeng, J., Chen, M., Guo, L., Lin, H., Mu, X., Fan, L., Zheng, M., Qiu, Y., 2019. Role of organic components in regulating denitrification in the coastal water of Daya Bay, southern. China. Environ. Sci. 21 (5), 831–844.
Zhou, R., Zeng, S., Hou, D., Liu, J., Weng, S., He, J., Huang, Z., 2019. Occurrence of human pathogenic bacteria carrying antibiotic resistance genes revealed by metagenomic approach: a case study from an aquatic environment. J. Environ. Sci. 80, 248–256.
Zilius, M., Bartoli, M., Bresciani, M., Katarzyte, M., Ruginis, T., Petkuviene, J., Lubiene, I., Giardino, C., Bukaveckas, P.A., de Wit, R., Razinkovas-Baziukas, A., 2014. Feedback Mechanisms Between Cyanobacterial Blooms, Transient Hypoxia, and Benthic Phosphorus Regeneration in Shallow Coastal Environments. Estuaries Coasts 37 (3), 680–694.
Zilius, M., Samuiloviene, A., Stanislauskienė, R., Broman, E., Bonaglia, S., Meškys, R., Zaiko, A., 2021. Depicting temporal, functional, and phylogenetic patterns in estuarine diazotrophic communities from eDNA and eRNA. Microb. Ecol. 81 (1), 36–51 (Under review).
Zilius, M., Vybernaite-Lubiene, I., Vaiciute, D., Petkuviene, J., Zemlys, P., Liskow, I., Voss, M., Bartoli, M., Bukaveckas, P.A., 2018. The influence of cyanobacteria blooms on the attenuation of nitrogen throughputs in a Baltic coastal lagoon. Biogeochemistry 141 (2), 143–165.